Electron-Phonon and Magnetoelastic Interactions in Ferromagnetic $Co[N(CN)_2]_2$

T. V. Brinzari,[1] J. T. Haraldsen,[2,3] P. Chen,[1] Q.-C. Sun,[1] Y. Kim,[4] L.-C. Tung,[4,*] A. P. Litvinchuk,[5] J. A. Schlueter,[6] D. Smirnov,[4] J. L. Manson,[7] J. Singleton,[8] and J. L. Musfeldt[1]

[1]*Department of Chemistry, University of Tennessee, Knoxville, Tennessee 37996, USA*
[2]*Theoretical Division, Los Alamos National Laboratory, Los Alamos, New Mexico 87545, USA*
[3]*Center for Integrated Nanotechnologies, Los Alamos National Laboratory, Los Alamos, New Mexico 87545, USA*
[4]*National High Magnetic Field Laboratory, Tallahassee, Florida 32310, USA*
[5]*Texas Center for Superconductivity and Department of Physics, University of Houston, Houston, Texas 77204, USA*
[6]*Materials Science Division, Argonne National Laboratory, Argonne, Illinois 60439, USA*
[7]*Department of Chemistry and Biochemistry, Eastern Washington University, Cheney, Washington 99004, USA*
[8]*National High Magnetic Field Laboratory, Los Alamos National Laboratory, Los Alamos, New Mexico 87545, USA*

(Received 9 January 2013; revised manuscript received 16 April 2013; published 24 July 2013)

We combined Raman and infrared vibrational spectroscopies with complementary lattice dynamics calculations and magnetization measurements to reveal the dynamic aspects of charge-lattice-spin coupling in $Co[N(CN)_2]_2$. Our work uncovers electron-phonon coupling as a magnetic field-driven avoided crossing of the low-lying Co^{2+} electronic excitation with two ligand phonons and a magnetoelastic effect that signals a flexible local CoN_6 environment. Their simultaneous presence indicates the ease with which energy is transferred over multiple length and time scales in this system.

DOI: 10.1103/PhysRevLett.111.047202 PACS numbers: 75.50.Xx, 63.20.kd, 63.70.+h, 75.80.+q

The exotic properties of multifunctional materials arise from a delicate balance between electronic, magnetic, and lattice degrees of freedom [1]. A key characteristic of these interactions is that they take place over multiple energy and time scales, making them influential in determining a variety of physical properties such as dc conductivity and crystal structure under static conditions [2] and electron-phonon and magnetoelastic coupling [3] under dynamic conditions. External stimuli like high magnetic field offer incisive opportunities to tune competing interactions. In rare cases, the size of the control parameter is large compared to the energy scales in the target material, a situation that suppresses intrinsic interactions and allows access to unusual areas of phase space where novel quantum effects can be revealed. In other instances, the control parameter is able to manipulate multiple interactions, a process that advances the microscopic understanding of coupling mechanisms. Both requirements are met in $Co[N(CN)_2]_2$, a system that heretofore has been recognized mainly for its chemical tunability and magnetoelastic coupling in the static limit [4–6].

As molecule-based materials are represented more and more among solids sporting unusual electronic and magnetic phenomena, spectroscopy is increasingly applied to explore the local dynamics of the complex building blocks and relate them to the macroscopic properties. This Letter chronicles a significant step in this direction, bringing together high field spectroscopy and magnetization with dynamics calculations and magnetic modeling to investigate energy transfer processes in $Co[N(CN)_2]_2$. Our work exposes rich charge-lattice-spin coupling manifested as (i) an avoided crossing between a field-dependent Co^{2+} crystal field excitation and low frequency wagging phonons that we discuss in terms of electron-phonon interactions and (ii) magnetoelastic effects in which the local Co^{2+} environment distorts and the $C{\equiv}N$ environment relaxes in response to an applied field. Although these mixing processes are most easily investigated in low energy scale materials like $Co[N(CN)_2]_2$, similar energy transfer mechanisms are relevant in higher energy scale compounds like the oxides. As an example, we discuss prospects for concurrent dynamic coupling in the cobaltites [7], where lattice flexibility and mixing between phonons and the electronic and spin degrees of freedom link a number of macroscopic and microscopic properties.

Polycrystalline α-$Co[N(CN)_2]_2$ was prepared as described previously [5]. Isothermal magnetization was measured at the National High Magnetic Field Laboratory (NHMFL) with a 65 T short-pulse magnet [8]. Fits to the magnetization and the calculated magnon dispersion were carried out using a mean-field approximation (see the Supplemental Material [9]). High field spectroscopies were performed at the NHMFL (4.2–40 K, 0–35 T, 0.5–1 cm^{-1} resolution). Lattice dynamics calculations on the Mn analog allowed assignment of the phonons [10].

Figure 1(a) displays the characteristic magnetic hysteresis loop of $Co[N(CN)_2]_2$ below the 9 K ferromagnetic transition [5]. Measurements in fields up to 60 T [Figs. 1(b)–1(d)] reveal an initial rapid rise of the magnetization (in fields of a few tesla) followed by a steady increase and approach to saturation. This behavior can be understood in terms of (i) conventional domain alignment processes followed by (ii) a field-induced quenching of the single-ion anisotropy and (iii) a subsequent increase of the spontaneous

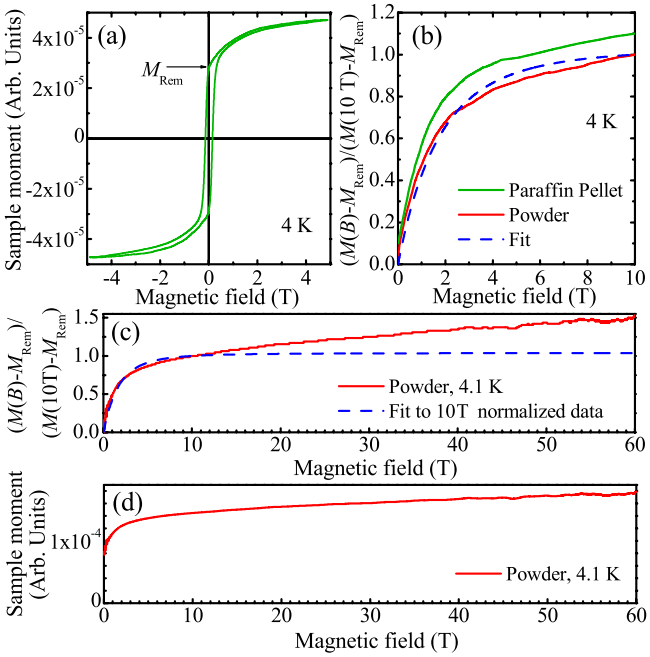

FIG. 1 (color online). (a) Magnetic hysteresis loop of $Co[N(CN)_2]_2$ in paraffin measured below the 9 K ferromagnetic transition. (b) Normalized magnetization for polycrystalline $Co[N(CN)_2]_2$ along with a theoretical fit up to 10 T. The paraffin pellet data (offset for clarity) are also shown. (c) Normalized magnetization of a powder sample along with our model fit up to 60 T displaying a quasilinear slope after ≃10 T that rises above the $S' = 1/2$ magnetization threshold as a result of the population of $M_{S'} = -3/2$ spin state. (d) Absolute magnetization of polycrystalline $Co[N(CN)_2]_2$ in fields up to 60 T.

magnetization [11]. We extract the anisotropy by fitting the magnetization below 10 T with a classical expansion of the Heisenberg Hamiltonian,

$$\mathcal{H} = -\frac{1}{2}\sum_{i\neq j} J_{ij}\mathbf{S}_i \cdot \mathbf{S}_j - D\sum_i \mathbf{S}_{iz}^2 - g\mu_B B\sum_i \mathbf{S}_{iz}, \quad (1)$$

where $J \simeq 4$ K is the exchange interaction [12], D is the anisotropy energy, g is the electron g factor, $\mathbf{S}_i$ is the local moment on site i, and B is the external magnetic field [13]. This choice to fit the low field magnetization to the $S' = 1/2$ ground state solution excludes excited states from the analysis, providing a distinct crossover point when the anisotropy is quenched, and distinguishes the field dependence of the excited states from that in the ground state (see the Supplemental Material [9]). This allows us to determine $D = 12 \pm 4$ cm^{-1}, a direct consequence of the large Co^{2+} spin-orbit coupling and crystal-field effects. For an octahedrally coordinated Co^{2+} center, the ground state level is $^4T_{1g}$ ($L = 1$ is only partially quenched). At ambient conditions, the Co^{2+} ion resides in the center of an axially elongated octahedron with $[N(CN)_2]^-$ ligands coordinated via nitrile nitrogens in the equatorial plane and via amide nitrogens in the axial direction [5]. Tetragonal distortion combined with

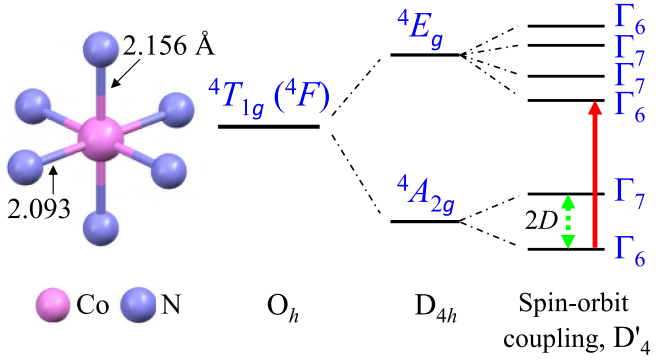

FIG. 2 (color online). Local geometry around the Co^{2+} magnetic center at 1.6 K [12] along with a schematic energy level diagram for the electronic states. The degeneracy of the Kramers doublets is further removed by exchange and/or external magnetic field. The latter is the Zeeman effect. Here, D is the anisotropy (12 ± 4 cm^{-1}) extracted from our magnetization measurements. The red (solid) arrow shows a plausible candidate for the 114 ± 5 cm^{-1} excitation in the Raman spectrum.

spin-orbit coupling acts to split the $^4T_{1g}$ term, producing a manifold of six Kramers doublets (Fig. 2). The two lowest doublets are Γ_6 ($M_{S'} = \pm 1/2$) and Γ_7 ($M_{S'} = \pm 3/2$) [14]. Although the true site symmetry of Co^{2+} ion is C_{2h}, we use D_{4h} to a good approximation [9]. Previous work demonstrates that only the lowest energy doublet (Γ_6) is populated at base temperature [12]. At 4 K, $Co[N(CN)_2]_2$ is therefore an effective $S' = 1/2$ system [12], and a strong magnetic field aligns the spins by slowly overcoming the anisotropy. Magnetization continues to increase at higher fields due to partial population of the higher energy $M_{S'} = -3/2$ branch of the Kramers doublet [5]. To further investigate the magnetic properties, we employed these parameters (J, D, S') along with $g = 5.34$ [12] to calculate the magnon dispersion of $Co[N(CN)_2]_2$. Using a mean-field approximation, we find a zone center one-magnon energy of 12 ± 4 cm^{-1} [9].

Figure 3(a) displays the magneto-Raman spectrum of $Co[N(CN)_2]_2$ in the low frequency range. We assign the peaks near 147 and 158 cm^{-1} as phonons with Co-$N_{ax}C_{(2)}$ and Co-$N_{eq(2)}$ wagging motion, respectively (Table I). Figure 3(b) summarizes the frequency vs. field trends of these phonons along with the behavior of a strongly field-dependent feature that we assign (below) as a Co^{2+} crystal field excitation. Taken together, these data reveal a dramatic avoided crossing. The sequence of events can be summarized as follows. At low fields, the phonons harden systematically, with 0.6 and 0.3 cm^{-1} frequency shifts at 14 T, respectively. Then a new feature appears in the spectrum. Initially, this structure has very weak intensity but becomes more pronounced as it shifts to higher frequency and interacts with the phonons. A closer look at intensity and integrated area trends demonstrates that this developing feature gains intensity by stealing it from the 147 and 158 cm^{-1} phonons while total oscillator strength remains approximately conserved. Near 18.5 T,

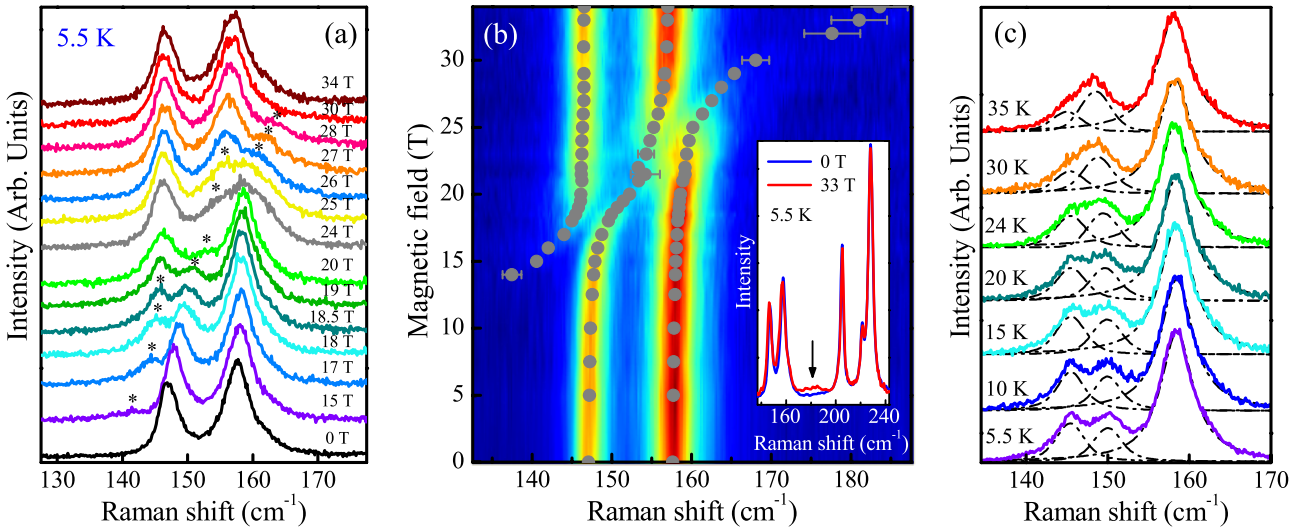

FIG. 3 (color online). (a) Representative magneto-Raman spectra of $Co[N(CN)_2]_2$ in fields up to 34 T at $T = 5.5$ K. The strongly field dependent feature that we assign as a Co^{2+} electronic excitation is marked with an asterisk, and the data are offset for clarity. (b) Contour plot of peak intensities as a function of frequency and magnetic field: blue is low intensity, red is high intensity. Dark gray points represent positions extracted by a peak fitting technique. Error bars are on the order of symbol size or as indicated. The inset shows an expanded view of the low temperature Raman spectrum along with the development of the broad structure as it approaches higher energy phonons. (c) Temperature dependence of the magneto-Raman spectrum at 18.6 ± 0.1 T. Black (dashed) lines are peak fits tracking the behavior of the Co^{2+} electronic excitation.

intensity is shared between the 147 cm^{-1} phonon and the new feature, and clear peak repulsion is observed [15]. Once the field-dependent structure moves out of range, the 147 cm^{-1} phonon recovers its strength and red shifts from its zero-field position (Table I). With increasing field, we find a heavily mixed phase with a temporary intensity loss and subsequent recovery of the field-dependent structure as it approaches the 158 cm^{-1} phonon. Mixing and crossing with the second phonon is similar to that of the first, with the maximum interaction taking place near 25 T. At higher field, the intensity of the hybrid Co^{2+} crystal field excitation diminishes, becoming very difficult to track above 30 T. It is likely that at even larger fields, this structure reappears and interacts with the next available phonon near $\simeq 205$ cm^{-1}. A small feature is indeed seen in our high field spectrum near 180 cm^{-1} [inset, Fig. 3(b)], but the weak intensity precludes further discussion.

To understand the nature of the structure that interacts strongly with the phonons, we begin by establishing a few facts. Based upon the observation that no other phonons in our investigated frequency and field range experience similar behavior, we attribute intensity enhancement and avoided crossing to the energetic proximity of the field-dependent structure to the 147 and 158 cm^{-1} phonons. Moreover, the field-induced blue shift of this structure is exceptionally large as compared to the behavior of

TABLE I. Assignment of selected vibrational peaks for $Co[N(CN)_2]_2$ along with their magnitude of change in a 35 T magnetic field at low temperature. The frequencies, symmetries, and displacement patterns are based upon calculations for the isostructural $Mn[N(CN)_2]_2$ analog (space group *Pnnm*, [10]).

Frequency (cm^{-1})	Symmetry	Vibrational mode assignment	$\lvert\Delta\alpha\rvert/\alpha$	Behavior with field
147^{R}	B_{1g}	Co-$N_{ax}C_{(2)}$ wagging type (N_{ax}, C motion in *ab* plane; modulates N_{ax}-Co-N_{eq} angle)		avoided crossing, softening at 34 T (~0.5 cm^{-1})
158^{R}	B_{2g}	Co-$N_{eq(2)}$ wagging (N_{eq} motion along *b*) (alternatively, N_{eq}-Co-N_{eq} rocking)		
289^{IR}	B_{2u}	$\sim\nu$(Co-N_{ax}) + $\sim\nu$(Co-N_{eq}) with ligand component	6%	harden, nonlinear
317^{IR}	$B_{1u}/B_{2u}/B_{3u}$	ligand bands, mostly N motion: scissors, twisting, wagging, rocking	4%	soften, nonlinear
995^{IR}		(NCN) bend, combination (IR + Raman)	2%	harden, quasilinear
1320^{IR}	B_{1u}	ν_{as} (N-C), in phase N motion along *c* axis	1%	soften, nonlinear
2294^{IR}	B_{2u}	ν_s (C≡N)	6%	soften, quasilinear

R is Raman-active, IR is infrared-active, ax is axial, and eq is equatorial.

phonons in $Co[N(CN)_2]_2$. From the frequency vs field data [Fig. 3(b)], we extract a slope $d\omega^*/dB$ of $\simeq 1.8$ cm^{-1}/T, where ω^* represents the frequency of the field-dependent structure. Extrapolating this trend to zero field, we estimate an unperturbed resonance frequency of 114 ± 5 cm^{-1}. Our magneto-Raman measurements do not, however, reveal a fundamental excitation in this range implying that either (i) the initial peak intensity is extremely weak or (ii) the fundamental excitation is Raman inactive and is activated only through coupling with nearby phonons.

The strikingly strong and quasilinear dependence of ω^* on magnetic field resembles the Zeeman effect suggesting either an electronic or magnetic excitation involving the Co^{2+} center. Energetic considerations combined with temperature studies, however, rule out scenarios involving a field-dependent magnon, multimagnon, or coupled magnon-phonon excitation (see the Supplemental Material [9]). We instead assign this structure as a Co^{2+} electronic excitation from the ground state Γ_6 level to the one of the higher lying doublets of the $^4T_{1g}$ term that moves with field as the Zeeman effect comes into play [16]. Such a candidate excitation is shown in Fig. 2. Unpublished neutron data [17] are consistent with the presence of a low energy electronic excitation between 80 and 120 cm^{-1}. Based on general symmetry considerations, $\Gamma_6 \rightarrow \Gamma_6$ and $\Gamma_6 \rightarrow \Gamma_7$ type excitations are Raman active, although in $Co[N(CN)_2]_2$, the intensity is weak at zero field and gains strength by mixing with the phonons. Using a two coupled oscillator model [15,18], we estimate the electron-phonon interaction energy to be on the order of 2 and 3 cm^{-1} for the 147 and 158 cm^{-1} phonons, respectively [9]. By comparison, electron-phonon coupling manifests itself in $CoBr_2$ and $FeCl_2$ [19,20] with mixed oscillator strengths and/or linewidths and coupling constants on the order of 8 cm^{-1}. The temperature dependence of the magneto-Raman response is in line with our assignment of the 114 cm^{-1} feature as an electronic excitation. Measurements at 18.6 T reveal that ω^* persists up to at least 35–40 K and displays no sensitivity to the 9 K Curie temperature [Fig. 3(c) and the Supplemental Material [9]], findings that exclude mechanistic scenarios involving magnons. The suppressed intensity of the 114 cm^{-1} electronic excitation at high temperature likely results from thermal broadening effects and a decreased population of the ground state level as the zero-field splitting is slowly overcome (Fig. 2) [18–21]. Lastly, we point out that cobalt-containing oxides are ideal systems with which to test the generality of this mechanism because they display low-lying electronic excitations, a rich array of phonons of different symmetries, and magnetism on the transition metal (and also rare earth) centers [7]. We anticipate strong, tunable electron-phonon coupling any time electronic terms are split and in energetic proximity to phonons of proper symmetry.

To investigate the interplay between local structure and magnetism, we also measured the magnetoinfrared response of $Co[N(CN)_2]_2$. Five phonons are sensitive to the field. Figure 4 summarizes our findings, and Table I provides the symmetry and mode assignments along with the size of the field-induced changes in the vibrational response [as measured by the relative absorption difference $|\Delta\alpha|/\alpha = |\alpha(35\text{ T}) - \alpha(0\text{ T})|/\alpha(0\text{ T})$]. The latter allows us to

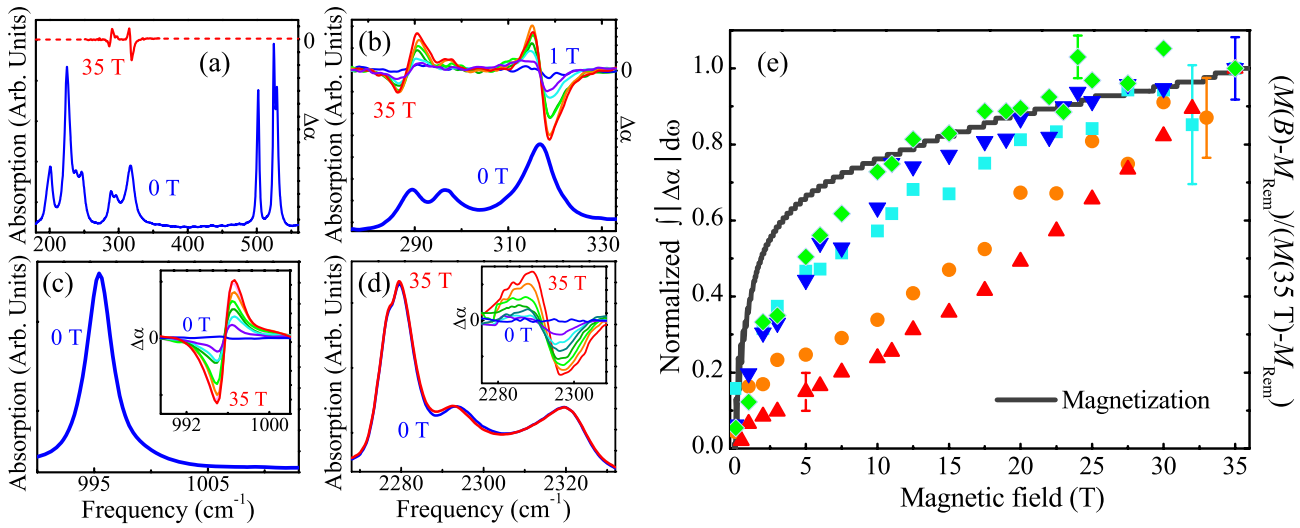

FIG. 4 (color online). (a) Far infrared absorption spectrum of $Co[N(CN)_2]_2$ along with the full field absorption difference, $\Delta\alpha = \alpha(35\text{ T}) - \alpha(0\text{ T})$. The absorption difference emphasizes field-induced changes. (b), (c), (d) Close-up views of selected modes at $B = 0$ and/or 35 T along with their absorption differences $\Delta\alpha = \alpha(B) - \alpha(0\text{ T})$. For (b), $B = 1, 3, 5, 10, 15, 25, 35$ T. For the insets of (c) and (d), $B = 0, 5, 10, 15, 20, 25, 30, 35$ T. (e) Integrated absolute absorption difference as a function of applied field compared with the magnetization. These data have been normalized at 35 T for display purposes. The field-dependent vibrational features show either linear or nonlinear growth with field depending on mode character. Inverted triangles: 289 cm^{-1} peak, diamonds: 317 cm^{-1}, circles: 995 cm^{-1}, squares: 1320 cm^{-1}, and regular triangles: 2294 cm^{-1} peak. All spectra were collected at 4.2 K.

identify the most important contributions to the field-induced local structure deformation. The infrared-active modes at 289 cm^{-1} (the Co-$N_{ax/eq}$ stretch) and 2294 cm^{-1} (the C≡N stretch) change by 6% between 0 and 35 T. Using a simple bond distance-frequency correlation, hardening of the 289 cm^{-1} phonon suggests slight axial compression of the CoN_6 octahedron, while simultaneous softening of the 2294 cm^{-1} mode indicates a more relaxed ligand environment that likely accommodates the need for distortion around the magnetic center. Other Co^{2+}-containing materials [7] may also display enhanced magnetoelastic coupling, the analysis of which can reveal how the local dynamics of the complex building blocks impacts the macroscopic properties. These field-induced local lattice deformations have a counterpart in magnetostriction [9,22].

To summarize, we combined high field Raman and infrared spectroscopies, lattice dynamics calculations, and magnetization to investigate energy transfer processes in $Co[N(CN)_2]_2$. Our analysis focuses on two classic signatures of coupling: (i) electron-phonon in which a crystal field excitation interacts with the phonons and (ii) magnetoelastic in which magnetostriction effects manifest themselves in the microscopic phonon response. That these two very different mixing processes are brought together in the same material illustrates the exceptional flexibility of the lattice and the ease with which energy can be transferred between the phonons and the electronic and spin degrees of freedom. Similar charge-lattice-spin interaction mechanisms are likely to be present in higher energy scale cobaltites and should prove useful in linking macroscopic and microscopic behavior in Co^{2+}-containing materials.

Research supported by the National Science Foundation under DMR-1063880 (J. L. M., UT), DMR-1005825 (J. L. M., EWU), DMR-0654118 (NHMFL), the U.S. Department of Energy (NHMFL), DE-AC52-06NA25396 and the center for integrated nanotechnologies (an Office of Science User Facility) (J. T. H.), DE-AC02-06CH11357 (J. A. S.), the state of Florida (NHMFL), and the state of Texas through the Texas Center for Superconductivity (A. P. L., UH).

*Currently at Department of Physics and Astrophysics, University of North Dakota, Grand Forks, ND 58202, USA.

[1] S. W. Cheong and M. Mostovoy, Nat. Mater. **6**, 13 (2007); P. K. Siwach, H. K. Singh, and O. N. Srivastava, J. Phys. Condens. Matter **20**, 273201 (2008); D. N. Basov, R. D. Averitt, D. van der Marel, M. Dressel, and K. Haule, Rev. Mod. Phys. **83**, 471 (2011); T. T. A. Lummen *et al.*, in Multiferroics: Synthesis, Characterization and Applications, edited by R. Ramesh and M. Lane (Wiley, New York) (to be published).

[2] Y. Tokura, Phys. Today **56**, No. 7, 50 (2003); S. A. J. Kimber *et al.*, Nat. Mater. **8**, 471 (2009); M. Kim, X. M. Chen, X. Wang, C. S. Nelson, R. Budakian, P. Abbamonte, and S. L. Cooper, Phys. Rev. B **84**, 174424 (2011).

[3] O. Gunnarsson, Rev. Mod. Phys. **69**, 575 (1997); A. S. Mishchenko, Adv. Condens. Matter Phys. **2010**, 306106 (2010); D. M. Edwards, Adv. Phys. **51**, 1259 (2002); A. B. Sushkov, O. Tchernyshyov, W. Ratcliff II, S. W. Cheong, and H. D. Drew, Phys. Rev. Lett. **94**, 137202 (2005); J. L. Musfeldt, in *Magnetism: Molecules to Materials I: Models and Experiments*, edited by J. S. Miller and M. Drillon (Wiley-VCH, Weinheim, 2001), p. 95; Ch. Kant, F. Mayr, T. Rudolf, M. Schmidt, F. Schrettle, J. Deisenhofer, and A. Loidl, Eur. Phys. J. Special Topics **180**, 43 (2009).

[4] M. Kurmoo and C. J. Kepert, New J. Chem. **22**, 1515 (1998).

[5] J. L. Manson *et al.*, Chem. Mater. **10**, 2552 (1998).

[6] C. J. Nuttall, T. Takenobu, Y. Iwasa, and M. Kurmoo, Mol. Cryst. Liq. Cryst. **343**, 227 (2000); A. Lappas, A. S. Wills, M. A. Green, K. Prassides, and M. Kurmoo, Phys. Rev. B **67**, 144406 (2003).

[7] B. Raveau and Md. M. Seikh, *Cobalt Oxides: From Crystal Chemistry to Physics* (Wiley-VCH, Weinheim, 2012); N. B. Ivanova, S. G. Ovchinnikov, M. M. Korshunov, I. M. Eremin, and N. V. Kazak, Phys. Usp. **52**, 789 (2009).

[8] P. A. Goddard *et al.*, New J. Phys. **10**, 083025 (2008).

[9] See Supplemental Material at http://link.aps.org/supplemental/10.1103/PhysRevLett.111.047202.

[10] T. V. Brinzari *et al.*, Phys. Rev. Lett. **110**, 237202 (2013). In contrast, $Mn[N(CN)_2]_2$ is a canted antiferromagnet below $T_N \simeq 16$ K [6].

[11] E. W. Lee, Rep. Prog. Phys. **18**, 184 (1955).

[12] C. R. Kmety, J. L Manson, S. McCall, J. E. Crow, K. L. Stevenson, and A. J. Epstein, J. Magn. Magn. Mater. **248**, 52 (2002).

[13] J. T. Haraldsen and R. S. Fishman, J. Phys. Condens. Matter **21**, 216001 (2009).

[14] O. Kahn, *Molecular Magnetism* (VCH, New York, 1993).

[15] W. Frank and P. von Brentano, Am. J. Phys. **62**, 706 (1994).

[16] The energy shift in magnetic field is $\delta E = g\mu_B M_{S'} B B_r(x)$, where $B_r(x)$ is the Brillouin function with $x \equiv (g\mu_B BS'/k_B T)$, and k_B and T are Boltzmann constant and temperature, respectively. For example, for the ground level Γ_6 ($M_{S'} = \pm 1/2$), $\delta E = 42$ cm^{-1} at $B = 34$ T ($g = 5.34$). The other contribution to the shift comes from splitting of the higher energy levels.

[17] J. L. Manson *et al.* (unpublished).

[18] T. D. Kang, E. Standard, K. H. Ahn, A. A. Sirenko, G. L. Carr, S. Park, Y. J. Choi, M. Ramazanoglu, V. Kiryukhin, and S.-W. Cheong, Phys. Rev. B **82**, 014414 (2010).

[19] D. J. Lockwood, G. Mischler, M. C. Schmidt, and I. W. Johnstone, J. Phys. C **12**, 1955 (1979).

[20] I. W. Johnstone, J. R. Fletcher, C. A. Bates, D. J. Lockwood, and G. Mischler, J. Phys. C **11**, 4425 (1978).

[21] H. Rho, M. V. Klein, and P. C. Canfield, Phys. Rev. B **69**, 144420 (2004).

[22] *Magnetism: Fundamentals*, edited by E. du Trémolet de Lacheisserie, D. Gignoux, and M. Schlenker (Springer Science, Boston, 2005).